Material Selection and Fabrication Parameters for Antireflective Nanostructures Integrated with Multijunction Photovoltaics

Emmett E. Perl[1], William E. McMahon[2], John E. Bowers[1], and Daniel J. Friedman[2]

[1]University of California at Santa Barbara, Santa Barbara, CA, 93106, USA
[2]National Renewable Energy Laboratory, Golden, CO, 80401, USA

Abstract — **Multijunction photovoltaic devices with four or more junctions require low reflection over a wavelength range that is nearly 50% wider than what is required for a triple-junction design. Antireflective nanostructures can drastically reduce reflection across this range; however careful design is necessary for integration with multijunction devices. In this work, we address the design trade-offs imposed by material availability by modeling absorption and reflection loss for various configurations. We find that the best performance is obtained using a hybrid design that combines antireflective nanostructures with a thin-film optical coating. Our models show that this configuration can increase transmitted power into the solar cell by 2.1% compared to the best standalone nanostructure configuration and 1.3% compared to an optimal thin-film antireflection coating. We also detail a fabrication process for integrating this hybrid design onto an active photovoltaic device.**

Index Terms — **biomimetics, III-V semiconductor materials, nanophotonics, optical films, photovoltaic cells, solar energy.**

I. INTRODUCTION

The efficiencies of multijunction photovoltaic devices far exceed those of single-junction designs. Champion cells have attained efficiencies greater than 44% under concentration and 38% at 1-sun, exceeding the Shockley-Queisser limit for single p-n junction devices. [1][2]

Multijunction designs with three subcells are currently used for concentrated photovoltaics (CPV) and space photovoltaics, where cell efficiency is critically important. One of the best methods for reducing the cost of these systems is to increase the efficiency of the photovoltaic device. For this reason, multijunction designs with four or more subcells are being rapidly developed. [3]-[6]

As the field moves beyond triple-junction (3-J) devices, optical design becomes more difficult. These solar cells require high transmission of light with wavelengths between roughly 300 and 1800 nm, a range that is nearly 50% wider than what is required for today's best 3-J devices. This places high importance on broadband reflection control. [7]-[9]

Antireflective (AR) nanostructures have demonstrated very low broadband reflectance and have been proposed as an alternative to thin-film AR coatings. [9]-[12] These designs consist of structures with sub-wavelength lateral dimensions, which suppress all but zero[th] order diffraction. When the nanostructure height is greater than half the wavelength of incoming light, all phases are present in the reflected beam and destructive interference yields near-zero net reflectance.

The nanostructures will exhibit broadband AR properties as long as this condition is met for the longest wavelength absorbed. [13][14]

Unfortunately, it is difficult to integrate AR nanostructures with multijunction photovoltaics without introducing new loss mechanisms. Direct patterning of the electrically active layers often leads to cell damage in the form of a reduced fill factor and open circuit voltage. [15] For nanostructures placed on top of the device, performance is limited by material constraints; nanostructures composed of high-index materials will absorb a significant amount of light while nanostructures composed of low-absorption materials will have a lower refractive index than the III-V active layers, and will thus induce a large Fresnel reflection loss at the III-V interface. [16]

In this work, we explore the design trade-offs imposed by material availability by modeling reflectance, absorptance, and transmittance for various AR nanostructure configurations placed onto a four-junction (4-J) photovoltaic device. [16][17]. Fig. 1 shows a diagram of the designs analyzed in this study.
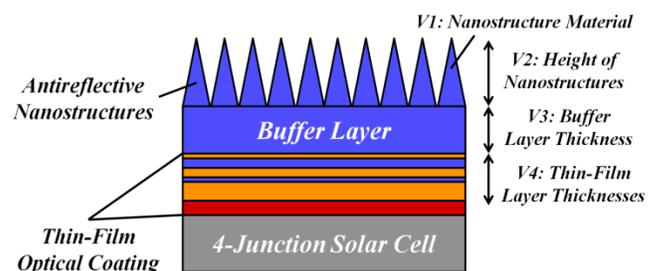
Fig. 1. Diagram showing the antireflective nanostructure designs analyzed in this paper. The four variables that are allowed to change (*V1-V4*) are shown on the right.

Four variables are allowed to change in the design: 1) the nanostructure material, 2) the height of the nanostructures, 3) the thickness of the buffer layer, and 4) the thickness of the layers in an underlying thin-film optical coating.

Each of these four variables has an effect on the AR properties of the system, and important limiting cases exist. When the nanostructure height is zero, the design becomes that of a conventional thin-film AR coating. Configurations where the thin-film layer thicknesses are zero correspond to standalone AR nanostructure designs. When the buffer layer thickness becomes larger than the coherence length of incoming light, the thin-film coating and the nanostructures

become optically decoupled and the configuration closely resembles that of a typical CPV or space photovoltaic system.

These design considerations are essential, but not sufficient. Antireflective nanostructures also require a fabrication process that does not damage the solar cell. For nanostructures placed directly on top of a device, process related damage can occur during a nanoimprinting or dry etching step. There are also challenges to developing a nanoimprinting process that is compatible with solar cells that have existing surface features, such as contact grids.

The objective of this work is to explore the practicality of various AR nanostructure configurations and to provide design guidance for their integration with multijunction photovoltaics.

II. OPTICAL MODELS

In this study, we compare the performance of various configurations that utilize either thin-film optical coatings, AR nanostructures, or both. More details on the design rules for thin-film optical coatings and AR nanostructures are reported elsewhere. [8][14][16][18]-[20]

A. Design of the Thin-Film Coating and AR Nanostructures

Thin-film AR coatings consisting of alternating layers of high- and low-index materials can attain near optimal performance for photovoltaic applications. [8][16][19][21] To maximize the power transmitted into the device, it is necessary that these layers do not absorb a significant amount of incoming sunlight. Tantalum pentoxide (Ta_2O_5) and silicon dioxide (SiO_2) form a good combination.

Additionally, transmission into the underlying solar cell can be maximized for designs that have a higher index material, such as titanium dioxide (TiO_2), adjacent to the III-V active layers, even when it has a non-zero extinction coefficient at short wavelengths. [16] The starting point for all the thin-film designs in this paper is a structure consisting of a single layer of TiO_2 and four alternating pairs of Ta_2O_5/SiO_2. [8][16][21]

The layer thicknesses are chosen to maximize transmitted power into a 4-J device consisting of a 20 nm thick aluminum indium phosphide ($AlInP_2$) "window" layer adjacent to a thick (~1 μm) indium gallium phosphide ($InGaP_2$) top junction. [7] Designs are found using a global search and simplex optimization, which minimize a merit function describing the quality of the design. The merit function is described by (1):

$$F = \int_{\lambda_L}^{\lambda_H} P(\lambda)*[1-T(\lambda)]d\lambda \qquad (1)$$

Where λ_L is the short wavelength cutoff of the device, λ_H is the long wavelength cutoff, $P(\lambda)$ describes the power in the AM1.5D spectrum, and $T(\lambda)$ is the modeled transmission into the InGaP top junction. λ_L and λ_H are chosen to be 300 and 1675 nm respectively, corresponding to a 4-J design with a

0.74 eV indium gallium arsenide (InGaAs) bottom junction grown lattice matched to indium phosphide (InP). [17]

The AR nanostructures are modeled by splitting them into 100 thin horizontal slices, then using Volume Averaging Theory to calculate the effective refractive index and extinction coefficient of each slice. [9][14][18] The height of the nanostructures is varied from 0-1500 nm, and a quintic-index profile is used since this has been shown to be near-ideal. [19] Nanostructures consisting of $AlInP_2$, gallium phosphide (GaP), zinc sulfide (ZnS), TiO_2, Ta_2O_5, and SiO_2 are considered. All optical constants are obtained using spectral ellipsometry or from the Sopra optical database. [22]

Fig. 2 shows the optimal layer thicknesses for hybrid designs that utilize both thin-film optical coatings and AR nanostructures composed of (a) SiO_2 or (b) Ta_2O_5.
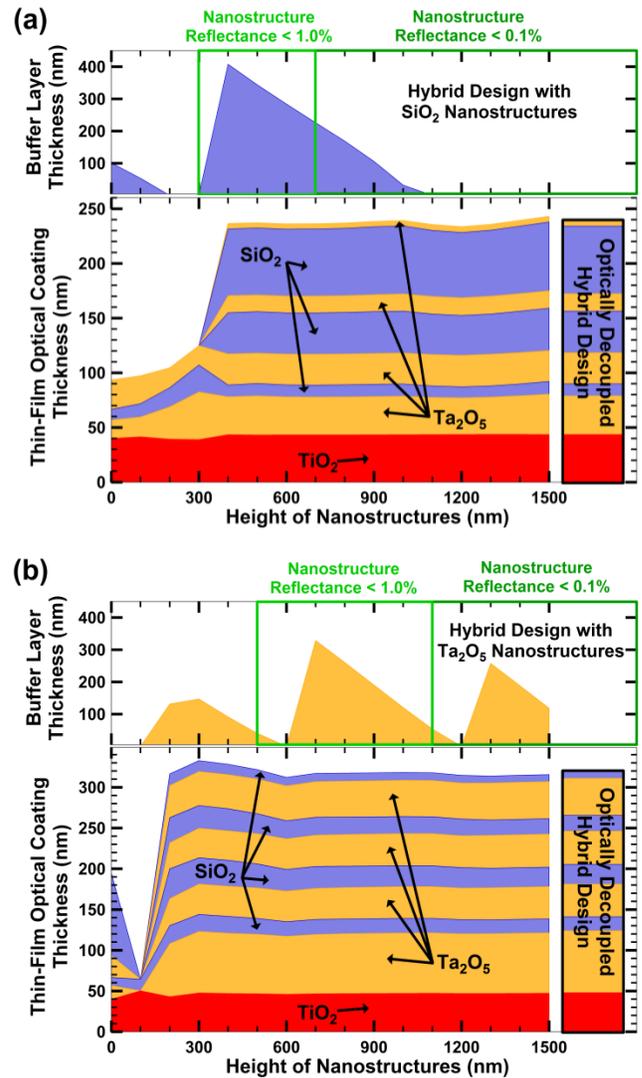
Fig. 2. Plots showing the cumulative thin-film and buffer layer thicknesses for hybrid designs with (a) SiO_2 and (b) Ta_2O_5 nanostructures. An optically decoupled design is shown on the right.

STANDALONE AR NANOSTRUCTURE COMPARISON

Nanostructure Material	Nanostructure Height	Reflected Power	Absorbed Power	Transmitted Power
AlInP$_2$	400 nm	4.1%	15.3%	80.6%
GaP	900 nm	1.6%	10.8%	87.6%
ZnS	700 nm	3.7%	5.7%	90.6%
TiO$_2$	800 nm	2.8%	4.6%	92.6%
Ta$_2$O$_5$	1500 nm	5.0%	3.2%	91.8%
SiO$_2$	200 nm	12.3%	2.7%	85.0%

These plots show how the optimal thin-film and buffer layer thicknesses change as the nanostructure height is varied. On the right, the optimal design is shown for the limiting case where the buffer layer is thicker than the coherence length of incoming light. This corresponds to a design where the nanostructures and the thin-film coating are optically decoupled, which would be the case for CPV receivers with secondary optics and space photovoltaic systems with glass coverslips. There are many interesting features in the optical design shown in these plots.

First, it is important to note that thin-film optical coatings with fewer layers often outperform more complex designs. This is seen in Fig. 2a for nanostructure heights less than 400 nm and Fig. 2b for nanostructure heights less than 200 nm. This behavior is related to the ideal refractive indices for a step-down interference coating. More details on this are reported elsewhere. [8][16]

Second, when the nanostructure reflectance is a fraction of one percent, the optimal layer thicknesses for a hybrid design are very similar to that of an optically decoupled design. When this is the case, reflectance from the nanostructures is low enough that it will not have a significant effect on the design of the thin-film AR coating.

Third, the thickness of the buffer layer oscillates until nanostructure reflectance is very low (< 0.1%), decreasing in thickness as the nanostructure height increases. The reason for this is that minimum reflectance occurs when the phase shift of light reflected off the first Ta$_2$O$_5$ interface is constant. [16]

B. Performance of the AR Nanostructure Designs

To compare the performance of the various AR nanostructure configurations, we model transmitted, absorbed, and reflected AM1.5D power as the nanostructure height is varied. These calculations help to quantify the tradeoff between material absorption for nanostructures composed of commonly available high-index materials and increased Fresnel reflections at the AlInP$_2$ "window layer" interface for nanostructures composed of commonly available low-absorption materials. In previous work, we showed that there is an excellent correlation between transmitted power into the top junction and modeled cell efficiency. [9][16]

Fig. 3 shows transmitted AM1.5D power for standalone AR nanostructures placed directly on top of a 4-J photovoltaic device. [17] Absorption is the limiting factor for nanostructures composed of AlInP$_2$ and GaP, which both absorb 400-500 nm light. For nanostructures composed of SiO$_2$, performance is limited by a large Fresnel reflection at the SiO$_2$/AlInP$_2$ interface.
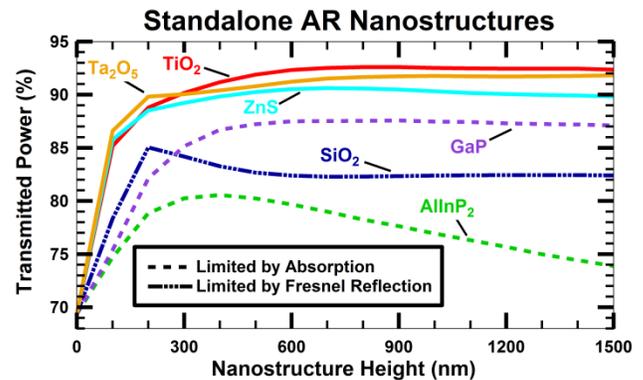
Fig. 3. Plot showing transmitted power for nanostructures composed of AlInP$_2$, GaP, ZnS, TiO$_2$, Ta$_2$O$_5$, and SiO$_2$.

Table I shows reflected, absorbed, and transmitted power when the nanostructure height is optimal for each design. Absorption loss is very significant for the AlInP$_2$ and GaP nanostructures.

Also note that for the SiO$_2$ nanostructures, the optimal feature height is just 200 nm. In this case, the nanostructured layer acts more like a thin-film AR coating with a reflectance minimum between 500-700 nm, a wavelength range corresponding to high AM1.5D power.

Fig. 4 compares transmitted AM1.5D power for three hybrid AR configurations and standalone TiO$_2$ nanostructures.
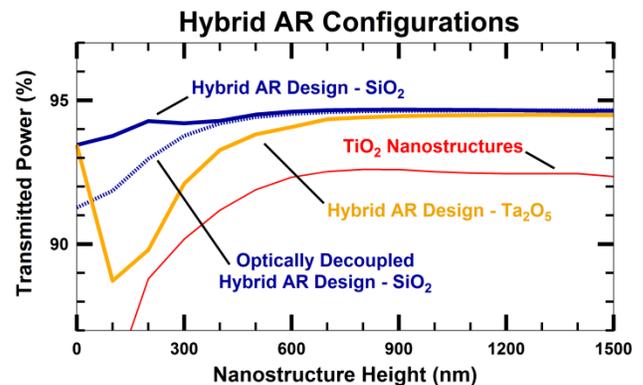
Fig. 4. Plot showing transmitted power for three hybrid AR designs and standalone TiO$_2$ nanostructures.

TABLE II
HYBRID AR COATING COMPARISONS

Hybrid Configuration	Nanostructure Height	Reflected Power	Absorbed Power	Transmitted Power
SiO$_2$ Hybrid AR Coating	900 nm	1.8%	3.5%	94.7%
Ta$_2$O$_5$ Hybrid AR Coating	1300 nm	2.0%	3.5%	94.5%
Optically Decoupled SiO$_2$ Hybrid	1500 nm	1.9%	3.5%	94.6%
TiO$_2$ Nanostructures	800 nm	2.8%	4.6%	92.6%
Optimal Thin-Film AR Coating	0 nm	3.2%	3.4%	93.4%

The blue lines show transmission for the SiO$_2$ hybrid AR designs from Fig. 2a, where the dotted line is for the case where the nanostructures and the thin-film optical coating are optically decoupled. Note that the optically coupled hybrid design maintains higher transmission until a nanostructure height of about 400 nm is obtained.

The orange line shows the Ta$_2$O$_5$ hybrid AR design from Fig. 2b. The initial drop in transmitted power from 0-100 nm is due to high reflectance in the short Ta$_2$O$_5$ nanostructures.

Table II shows reflected, absorbed, and transmitted power when the nanostructure height is optimal for each AR design shown in Fig. 4. The performance of an optimized thin-film AR coating is also shown for comparison.

The best performance is achieved by the three hybrid designs which combine AR nanostructures with thin-film optical coatings. Transmitted power for each configuration is comparable when the nanostructure height becomes large.

Transmission for both optically coupled and decoupled hybrid AR designs with SiO$_2$ nanostructures exceeds that of an optimized thin-film design by more than 1.0% when the nanostructure height is greater than 500 nm. This hybrid configuration therefore represents a promising pathway to increasing 4-J cell efficiency for optical designs with or without cover glass.

III. FABRICATION AND RESULTS

It is clear that there is a benefit to placing AR nanostructures onto a multijunction solar cell when they are also integrated with a thin-film optical coating.

However, fabrication of the nanostructures can be challenging. Cell damage can occur during an imprinting or dry etching step, which is often used to transfer the nanostructure onto the photovoltaic device. Furthermore, a processed cell will have contact grids and other topological features which make pattern transfer difficult.

Procedures for placing AR nanostructures onto the cover glass of a CPV or space photovoltaic system have been reported previously. [23][24] In this section, we will detail a fabrication process for placing an optically coupled hybrid AR design onto a representative gallium arsenide (GaAs) solar cell.

A. Fabrication of the Hybrid AR Design on an Active Device

As a preliminary investigation, an optically coupled hybrid AR design is placed onto two samples; one consisting of a layer of AlInP$_2$ grown on GaAs and the other an upright GaAs single-junction active photovoltaic device.

The single-junction device is first fabricated using III-V processing techniques. A gold (Au) back contact is deposited onto the backside of the GaAs substrate, then Au metal grids and contact pads are deposited onto the front surface of the sample. The GaAs contacting layer is removed to expose the underlying AlInP$_2$ window layer, and mesas are formed to isolate the cells. [7]

A thin-film optical coating is then deposited using a VEECO ion beam assisted sputter deposition system. Optical coatings consisting of only two thin-film materials (TiO$_2$ and SiO$_2$) were used during process development. An additional 1-2 μm of SiO$_2$ is deposited on top of the thin-film layers to accommodate the AR nanostructures. For imprinting, it is important that this SiO$_2$ layer rises above all other features on the sample. We mask off the metal grids and contact pads during deposition to ensure that this is the case.

The antireflective nanostructures are transferred to the sample using nanoimprint lithography (NIL). Thermal NIL is commonly used to transfer these types of patterns. However, this process requires high pressure (400-500 psi), high temperature (120-140°C), and often a hard stamp. [9] These high temperatures and pressures have the potential to damage the photovoltaic device.

An alternative process utilizes ultraviolet (UV) NIL. [25] With UV NIL, the imprinting process can be done at low pressure (2-10 psi), low temperature (20-30°C) and can more readily use a flexible imprinting stamp. Fig. 5 details the UV NIL process.
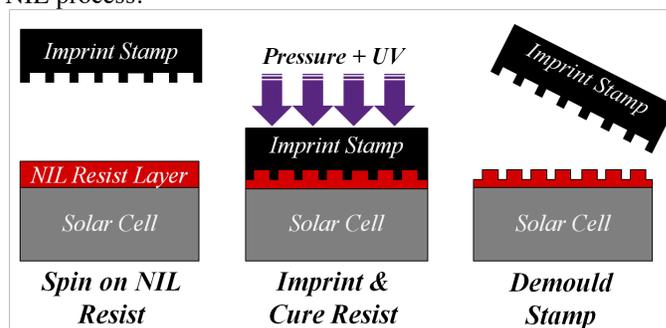
Fig. 5. Diagram of the UV NIL process used to transfer the AR nanostructures onto our samples.

AR nanostructures from a nickel imprinting stamp, fabricated by NIL Technology, are first transferred to a flexible and transparent polydimethylsiloxane (PDMS) sample

using OrmoStamp, a hybrid polymer developed by Micro Resist Technology. The flexible stamp allows for conformal imprinting even when the surface is not flat, as is the case for most solar cells. A perfluorodecyltrichlorosilane (FDTS) anti-stick treatment is then applied to the PDMS secondary stamp to assist with demoulding. [25]

A UV imprint resist (MR-UVCur21) is spin coated onto the sample, and the flexible PDMS stamp is placed pattern down onto the imprint resist. A Nanonex imprinting tool is used to carry out the imprinting process.

The sample is imprinted at a pressure of 5 psi for 2 minutes so that the UV imprint resist can fill the voids in the PDMS stamp. A UV lamp is then turned on for 20 seconds to cure the resist. After the NIL process is complete, the PDMS stamp is peeled off of the sample, leaving its negative image in the NIL resist layer. After imprinting, the nanostructures have a feature height and pitch of approximately 350 nm.

An inductively coupled plasma etch is then used to transfer the pattern to the underlying SiO_2 layer using a CHF_3 etch chemistry. The selectivity of resist:SiO_2 is approximately 1:2, allowing the feature height to increase to roughly 700 nm. After pattern transfer, the NIL resist layer is removed.

B. Results for the Hybrid AR Designs

The specular reflectance of a sample consisting of ~500 nm of $AlInP_2$ grown on a GaAs substrate is measured using a Cary 500 UV-VIS-NIR Spectrophotometer. Fig. 6 shows the measured and modeled reflectance of this sample with no AR coating and with a hybrid AR design placed onto it.
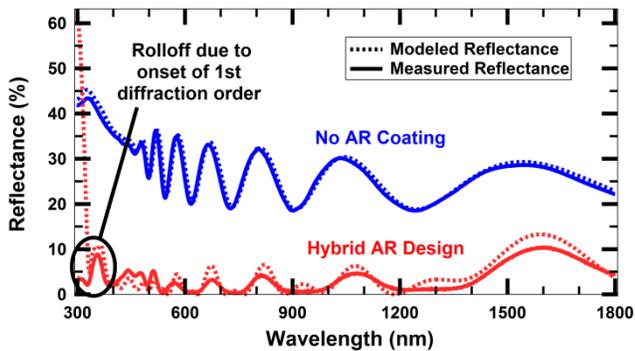
Fig. 6.   Plot showing the measured and modeled reflectance for an $AlInP_2$/GaAs sample with and without a hybrid AR design.

The measured AM1.5D reflected power is reduced from 27.5% for the uncoated sample to 2.6% for the sample with a hybrid AR design. There is also good agreement between the simulated and measured specular reflectance. This provides indirect evidence that the nanostructures are not scattering a significant amount of light through most of the solar spectrum.

For wavelengths shorter than 350 nm, we start to see a big variation between the modeled and measured specular reflectance. This occurs because the nanostructures begin to scatter and diffract light with wavelengths shorter than 350 nm, a size corresponding to the lateral dimensions of the features. [9][14][16][18] This results in attenuation for the measured reflectance but not the modeled reflectance.

Fig. 7 shows preliminary I-V characteristics for a single-junction GaAs solar cell before and after a hybrid AR design is fabricated.
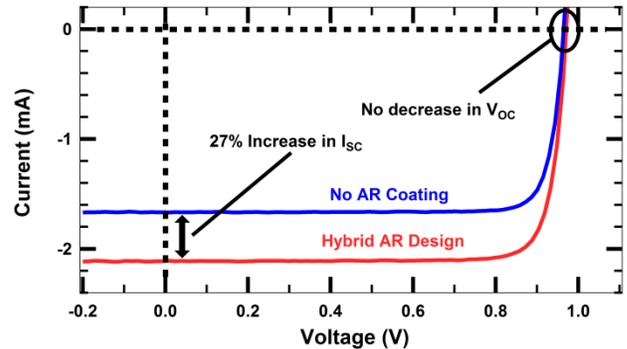
Fig. 7.   Plot showing the I-V characteristics of a single-junction GaAs cell before and after placing a hybrid AR design onto the cell.

We measure a 27% increase in the short circuit current (I_{SC}) compared to the uncoated device. Further improvements in I_{SC} are expected with a redesigned mask and reoptimized thin-film coating design. Additionally, note that there is small increase in the cell's open circuit voltage (V_{OC}). This is an indication that the fabrication process is not damaging the photovoltaic device.

IV. SUMMARY

In this work, we compare the performance of various AR nanostructure configurations by modeling reflectance, absorptance, and transmittance into a 4-J cell structure. We explore designs with different nanostructure materials and varying nanostructure heights. As these two variables are changed, the buffer layer and thin-film layer thicknesses are optimized for maximum transmitted power into the device.

We find that the best performing standalone AR nanostructure design is composed of TiO_2. While this design outperforms other standalone AR nanostructures, its performance remains lower than that of an optimal thin-film AR coating.

The primary challenge for these standalone AR nanostructure designs results from a lack of suitable materials with a low extinction coefficient and high refractive index. This leads to an unavoidable tradeoff between material absorption for nanostructures made of common high-index materials and increased Fresnel reflection at the $AlInP_2$ "window" layer interface for nanostructures made of common low-absorption materials.

We find that a hybrid design that integrates AR nanostructures with a thin-film optical coating can outperform an optimal thin-film AR coating. The hybrid design maintains low power reflection and low absorption across the solar spectrum, and optical models show that this approach can

increase transmitted power by approximately 2.1% compared to TiO$_2$ nanostructures and 1.3% compared to an optimal thin-film AR coating.

We also detail a fabrication process for placing the hybrid AR design onto an active photovoltaic device using a soft UV nanoimprint lithography process.

A hybrid AR design is fabricated on an AlInP$_2$/GaAs sample. After fabrication, the measured AM1.5D reflected power is reduced from 27.5% for the uncoated sample to 2.6%. Another hybrid AR design is placed onto a single-junction GaAs solar cell. An increase in short circuit current and open circuit voltage is observed, indicating that the fabrication process does not damage the cell. The integration of this hybrid AR design onto a 4-J photovoltaic device should result in a direct improvement in cell efficiency for next-generation multijunction photovoltaic devices.

REFERENCES

[1] M. A. Green, K. Emery, Y. Hishikawa, W. Warta, and E. D. Dunlop, "Solar cell efficiency tables (version 43)," *Progress Photovoltaics: Res. Appl.,* vol. 22, no. 1, pp. 1-9, 2014.

[2] W. Shockley and H. J. Queisser, "Detailed balance limit of efficiency of p-n junction solar cells," *Journal of Applied Physics*, vol. 32, no. 3, pp. 510-519, 1961.

[3] D. C. Law, R. R. King, H. Yoon, M. J. Archer, A. Boca, C. M. Fetzer, *et al.*, "Future technology pathways of terrestrial III-V multijunction solar cells for concentrator photovoltaic systems," *Solar Energy Materials and Solar Cells*, vol. 94, pp. 1314-1318, no. 8, 2010.

[4] F. Dimroth, M. Grave, P. Beutel, U. Fiedeler, C. Karcher, T. N. D. Tibbits, *et al.*, "Wafer bonded four-junction GaInP/GaAs//GaInAsP/GaInAs concentrator solar cells with 44.7% efficiency," *Progress Photovoltaics: Res. Appl.*, 2014.

[5] P. T. Chiu, D. C. Law, R. L. Woo, S. B. Singer, D. Bhusari, W. D. Hon, *et al.,* "Direct semiconductor bonded 5J cell for space and terrestrial applications," *IEEE J. Photovoltaics*, vol. 4, no. 1, pp. 493-497, 2014.

[6] P. Patel, D. Aiken, D. Chumney, A. Cornfeld, Y. Lin, C. Mackos, *et al.*, "Initial results of the monolithically grown six-junction inverted metamorphic multi-junction solar cell," in *Proc 38th IEEE Photovoltaic Spec. Conf.*, vol. 2, pp. 1-4, 2012.

[7] D. J. Friedman, J. M. Olson, and S. R. Kurtz, "High-efficiency III-V multijunction solar cells," in *Handbook of Photovoltaic Science and Engineering*, 2nd Ed., A. Luque and S. Hegedus, Eds., ed Chichester UK: Wiley, 2011, pp. 314-364.

[8] D. J. Aiken, "High performance anti-reflection coatings for broadband multi-junction solar cells," *Solar Energy Materials and Solar Cells,* vol. 64, no. 4, pp. 393-404, 2000.

[9] E. E. Perl, C.-T. Lin, W. E. McMahon, D. J. Friedman, and J. E. Bowers, "Ultra-Broadband & Wide-Angle Hybrid Antireflection Coatings with Nanostructures," *Journal of Photovoltaics,* vol. 4, no. 3, pp. 962-967, 2014.

[10] J. Tommila, V. Polojärvi, A. Aho, A. Tukiainen, J. Viheriälä, J. Salmi, *et al.*, "Nanostructured broadband antireflection coatings on AlInP fabricated by nanoimprint lithography," *Solar Energy Materials and Solar Cells*, vol. 94, no. 10, pp. 1845-1848, 2010.

[11] P. Yu, M.-Y. Chiu, C.-H. Chang, C.-Y. Hong, Y.-L. Tsai, H.-V. Han, *et al.*, "Towards high-efficiency multi-junction solar cells with biologically inspired nanosurfaces," *Progress Photovoltaics: Res. Appl.*, 2012.

[12] J. Tommila, A. Aho, A. Tukiainen, V. Polojärvi, J. Salmi, T. Niemi, *et al.*, "Moth-eye antireflection coating fabricated by nanoimprint lithography on 1 eV dilute nitride solar cell," *Progress Photovoltaics: Res. Appl.,* vol. 21, no. 1, pp. 1158-1162, 2013.

[13] C. G. Bernhard, "Structural and functional adaptation in a visual system," *Endeavor*, vol. 26, no. 98, pp. 79-84, 1967.

[14] S. J. Wilson, and M. C. Hutley, "The optical properties of moth eye antireflection surfaces," *Journal of Modern Optics*, vol. 29, no. 7, pp. 993-1009, 1982.

[15] J. Zhu, C.-M. Hsu, Z. Yu, S. Fan, and Y. Cui, "Nanodome solar cells with efficient light management and self-cleaning," *Nano Letters*, vol. 10, no. 6, pp. 1979-1984, 2009.

[16] E. E. Perl, W. E. McMahon, D. J. Friedman, and J. E. Bowers, "Design of antireflective nanostructures and optical coatings for next-generation multijunction photovoltaic devices," *Optics Express,* submitted.

[17] W. E. McMahon, C.-T. Lin, J. S. Ward, J. F. Geisz, M.W. Wanlass, J. J. Carapella, *et al.*, "Metal pillar interconnection topology for bonded two-terminal multijunction III-V solar cells," *Journal of Photovoltaics*, vol. 3, no. 2, pp. 868-872, 2013.

[18] D. G. Stavenga, S. Foletti, G. Palasantzas, and K. Arikawa, "Light on the moth-eye corneal nipple array of butterflies," in *Proc. Royal Society B: Biological Sciences,* vol. 273, no. 1587, pp. 661-667, 2006.

[19] W. H. Southwell, "Gradient-index antireflection coatings," *Optics Letters,* vol. 8, no. 11, pp. 584-586, 1983.

[20] H. A Macleod, *Thin-Film Optical Filters* (CRC Press, Boca Raton, Fla., 2001), Chap. 4.

[21] W. H. Southwell, "Coating design using very thin high- and low-index layers," *Applied Optics,* vol. 24, no. 4, pp. 457-460, 1985.

[22] Refractive Index Database (2011, December) Available: http://refractiveindex.info

[23] Y. M. Song, Y. Jeong, C. I Yeo, and Y. T. Lee, "Enhanced power generation in concentrated photovoltaics using broadband antireflective coverglasses with moth eye structures," *Optics Express*, vol. 20, no. 106, pp. A916-A923, 2012.

[24] J. W. Leem, J. S. Yu, J. Heo, W.-Kyu Park, J.-H, Park, W. J. Cho, and D. E. Kim, "Nanostructured encapsulation coverglasses with wide-angle broadband "antireflection and self-cleaning properties for III-V multi-junction solar cell applications," *Solar Energy Materials and Solar Cells*, vol. 120, pp. 555-560, 2014.

[25] J. Viheriälä, T. Niemi, J. Kontio, and M. Pessa, "Nanoimprint lithography - next generation nanopatterning methods for nanophotonics fabrication," in *Recent Optical and Photonic Technologies*, Chap. 14, 2010.